

Bayesian optimization for tuning and selecting hybrid-density functionals

R. A. Vargas-Hernández*

Department of Chemistry, University of British Columbia,
Vancouver, British Columbia, Canada, V6T 1Z1.

(Dated: December 15, 2024)

Hybrid-density functional methods such as, B3LYP are widely used across different fields to predict physical properties of molecular and material systems. The optimization of hybrid-density functionals is computationally demanding. The machine learning algorithm presented here, Bayesian optimization, is capable of optimizing efficiently the exchange-correlation constants for hybrid-density functionals and select the exchange-correlation functional that describes a benchmark data most accurately. Bayesian optimization is an iterative method that uses Gaussian process models to find the minimum of non-analytic functions. The same numerical procedure can be applied to other computational methods whose parameters can be tuned by comparison with benchmark data.

Introduction. Computational models in the fields of chemistry and physics are usually optimized using an error function that quantifies the accuracy of the models' prediction. The optimization of the models normally consists on finding the value of the parameters that best reproduce benchmark data or experimental measurements, such as energy barriers and atomization energies, to mention a few. The optimization of the density functional (DF) models using a set of molecular properties [1, 2] is one of the most common examples of the optimization of computational models using experimental data.

One of the most familiar types of error functions used in optimizing computational models is the *root mean square error* (RMSE) function,

$$\mathcal{L} = \sqrt{\frac{1}{|M|} \sum_{m_i} (R_{m_i}^{DFT} - R_{m_i}^{exact})^2}, \quad (1)$$

where $R_{m_i}^{DFT}$ is the physical property m_i computed with a DF method or any computational model; and $R_{m_i}^{exact}$ is the exact value. $|M|$ is the total number of physical properties used in the error function. The most common DF methods are the hybrid-density functionals, introduced by Becke [3, 4], which combine local and non-local treatments of exchange (X) and correlation (C) with Hartree-Fock (HF) exchange,

$$E_{XC}^{acm3} = E_{XC}^{LSD} + a_0(E_X^{exact} - E_X^{LSD}) + a_X(E_X^{GGA} - E_X^{LSD}) + a_C(E_C^{GGA} - E_C^{LSD}), \quad (2)$$

where a_0 , a_X and a_C are adjustable parameters, E_X^{GGA} and E_C^{GGA} are the generalized gradient approximation (GGA) exchange and correlation, and E_X^{LSD} is the local spin density (LSD) part. Since the value of $R_{m_i}^{DFT}$ depends on a_0 , a_X , a_C , E_X^{GGA} and E_C^{GGA} , the error function is also a function of these parameters,

$$\mathcal{L} = f(a_0, a_X, a_C; E_X, E_C). \quad (3)$$

The values of a_0 , a_X and a_C for a E_{XC} are typically optimized by minimizing \mathcal{L} with respect to a benchmark set of molecules or results from higher lever numerical

methods, $R_{m_i}^{exact}$. For example, the parameters of DF B3PW91 were optimized by considering an error function with 56 atomization energies (AEs), 42 ionization potentials (IPs), 8 proton affinities (PAs), and 10 first-row total atomic energies [3, 4].

Any analytical function like \mathcal{L} can be optimized using gradient-based methods [5, 6] by computing the change of \mathcal{L} with respect to its parameters, $\frac{\partial \mathcal{L}}{\partial a_i}$; in this case a_0 , a_X and a_C . While \mathcal{L} has a closed form, the gradient of $R_{m_i}^{DFT}$ with respect to any of XC coefficients does not have a simple analytical form since it also depends on the physical property chosen to evaluate the accuracy of E_{XC} , $\frac{\partial \mathcal{L}}{\partial a_i} \propto \frac{\partial R_{m_i}}{\partial a_i}$. Additionally, each evaluation of \mathcal{L} for different values of a_0 , a_X and a_C can take hours of computational time if $|M|$ is large or $R_{m_i}^{DFT}$ is related to a large molecule. The optimization of DF models is currently done using grid search, and scale with the number of points in the grid [2, 3, 7]. This is the bottleneck of parametrizing DF models.

Among the most important contributions the most important contributions of the machine learning (ML) field are the optimization methods designed to minimize complex functions to efficiently train ML models [5, 6]. ML algorithms have been demonstrated to be powerful numerical tools to simulate many-body physics [8–15]. For example, ML algorithms have also been applied to bypass the Kohn-Sham equations and reduce the computational complexity in DF calculations. [16–18]. Bayesian methods have also been applied to approximate and optimize the exchange-correlation for various systems [19–23]. The application of optimization algorithms already had a great impact in modern science by allowing us to tackle new problems, e.g. controlling a robot to do chemical synthesis [24, 25] or for the production of Bose-Einstein condensates [26]. In this contribution we demonstrated that parameters of DF models can be efficiently tuned to select the most accurate E_{XC} using ML algorithms.

It is assumed that ML algorithms, like Bayesian optimization (BO), can be used to optimize computational models like DF models in a more automated and efficient

manner. BO is one of the most common ML algorithms used to minimize non-analytic functions like Eq. 1 [27, 28]. More recently, BO was used in computational chemistry to generate low-energy molecular conformers [31], and to build global potential energy surfaces for reactive molecular systems using feedback from quantum scattering calculations [32]. The value of this result is clear since automation to improve physical models is one of the most important goals in computational physics and chemistry. Our method illustrates that one can efficiently tune the parameters of DFs to better describe a molecular system and select the most accurate E_{XC} form. In the following section we introduce the BO algorithm.

Method. Bayesian optimization is a sequential search algorithm designed to find the global minimizer (or maximizer) of an unknown non-analytic or oracle function,

$$\mathbf{x}^* = \arg \min_{\mathbf{x}} f(\mathbf{x}), \quad (4)$$

where \mathbf{x} is a continuous variable, $\mathbf{x} \in \mathbb{R}^\ell$.

BO requires two components: a model that approximates $f(\mathbf{x})$ and an acquisition function, $\alpha(\mathbf{x})$ [27, 28]. Here we use Gaussian process (GP) models as the probabilistic surrogate model to approximate $f(\mathbf{x})$ [30]. GP model is a non-parametric regression model that assumes that the training data, denoted as $\mathcal{D} = \{X, \mathbf{y}\}$, is jointly Gaussian distributed. The prediction of a new point using GP models is carried out by computing the conditional distribution of $f(\mathbf{x}_*)$ at the point we want to predict, \mathbf{x}_* . The conditional distribution has a closed form characterized by its mean, $\mu(\mathbf{x}_*)$, and standard deviation, $\sigma(\mathbf{x}_*)$,

$$\begin{aligned} \mu(\mathbf{x}^*) &= K(\mathbf{x}_*, X)^\top [K(X, X) + \sigma_n^2 I]^{-1} \mathbf{y} \\ \sigma(\mathbf{x}^*) &= K(\mathbf{x}_*, \mathbf{x}_*) \end{aligned} \quad (5)$$

$$-K(\mathbf{x}_*, X)^\top [K(X, X) + \sigma_n^2 I]^{-1} K(\mathbf{x}_*, X) \quad (6)$$

where $K(\cdot, \cdot)$ is the design or covariance matrix. The matrix elements of $K(\cdot, \cdot)$, $K_{i,j} = k(\mathbf{x}_i, \mathbf{x}_j)$, are computed with a kernel function. For this work we used the *radial basis function* (RBF) kernel,

$$k_{RBF}(\mathbf{x}_i, \mathbf{x}_j) = \exp\left(-\frac{1}{2}(\mathbf{x}_i - \mathbf{x}_j)^\top M(\mathbf{x}_i - \mathbf{x}_j)\right), \quad (7)$$

where M is a diagonal matrix that has different length-scale parameter, ℓ_d , for each dimension of \mathbf{x} . All ℓ_{dS} are described as θ . The parameters of the kernel function, θ , are optimized by maximizing the marginal log-likelihood,

$$\begin{aligned} \log p(\mathbf{y}|X, \theta) &= -\frac{1}{2} \mathbf{y}^\top K(X, X)^{-1} \mathbf{y} \\ &\quad -\frac{1}{2} \log |K(X, X)| - \frac{N}{2} \log(2\pi), \end{aligned} \quad (8)$$

where N is the total number of points in \mathcal{D} and $|K(X, X)|$ is the determinant of the design matrix. For more insight

on GP models, we encourage the reader to consult Ref. [30, 33].

The acquisition function is designed to quantify the informational gain if we evaluate f at a new point, $f(\mathbf{x}_{N+1})$. The goal of BO is to reduce the computational complexity of minimizing $f(\mathbf{x})$, by iteratively minimize $\alpha(\mathbf{x})$, which is less computationally demanding [27, 28]. Here, we only considered two acquisition functions: the *expected improvement* (EI),

$$\alpha_{EI}(\mathbf{x}) = (\mu(\mathbf{x}) - y_{max})\Phi(z(\mathbf{x}; y_{max})) + \sigma(\mathbf{x})\phi(z(\mathbf{x}; y_{max})), \quad (9)$$

where $z(\mathbf{x}; y_{min}) = (\mu(\mathbf{x}) - y_{min})/\sigma(\mathbf{x})$, $\Phi(\cdot)$ is the normal cumulative distribution and $\phi(\cdot)$ is the normal probability distribution. y_{min} is the minimum value observed in the training data, $y_{min} = \arg \min \mathbf{y}$. Secondly, we considered the *upper confidence bound* (UCB),

$$\alpha_{UCB}(\mathbf{x}) = \mu(\mathbf{x}) + \kappa\sigma(\mathbf{x}), \quad (10)$$

where κ is the exploration-exploitation constant. For all the results presented in this work we set $\kappa = 1$. For both acquisition functions, $\mu(\mathbf{x})$ and $\sigma(\mathbf{x})$ are the mean and the standard deviation from a GP model, Eqs. (5-6). By sequentially optimizing the acquisition function and evaluating \mathcal{L} in the proposed points, BO finds the minimum/maximum of the non-analytic function [29]. In the following sections, we illustrate how BO can be used to optimize the free parameters of computational physics models such as hybrid-density functionals.

Results. All the DF calculations are performed with the Gaussian 09 suite [40] and with the 6-31G(d) basis set. The molecular geometries used in the DF calculations were optimized with MP2/6-31G(d). The loss function we considered for the optimization of all the different DF models is the RMSE of the 32 atomization energies of the Gaussian-1 (G1) database [37–39], Eq. 1. First we optimized the free parameter, a_0 , of the PBE0 where, $a_X = 1 - a_0$ and $a_C = 1$ [34–36] using BO and UCB acquisition function with $\kappa = 1$. The BO algorithm found the minimum for \mathcal{L} , $a_0^* = 0.1502$, with only 6 total evaluations, and the RMSE = 10.08 kcal mol⁻¹. The value of the RMSE for the original PBE0 [35, 36], $a_0 \approx \frac{1}{4}$, is 11.30 kcal mol⁻¹ [29].

The second test we considered was the jointly optimization of the a_0, a_X and a_C for 30 different E_{XC} using BO; combination of 5 different *exchange* functionals [43], E_X , and 6 different *correlation* functionals [44]. For each E_{XC} we carried out 5 different optimizations with different initial points. The initial points used in the BO algorithm were 15, $N_0 = 5 \times d$, where d is the dimensionality of \mathcal{L} , $d = 3$. These points were sampled using the latin hyper cube sampling (LHS) algorithm [41] to avoid sampling multiple points close to each other. The lowest RMSE found by BO are displayed in Figure 1. For each

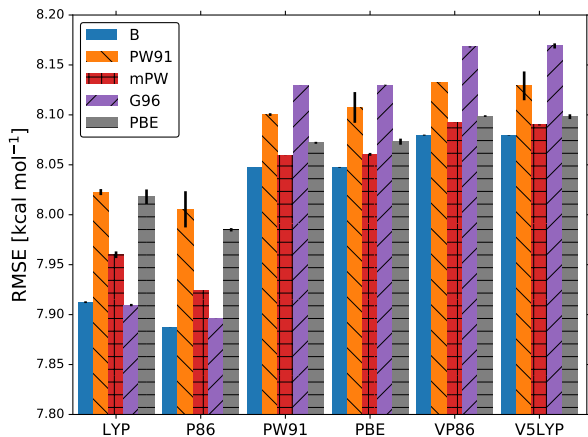
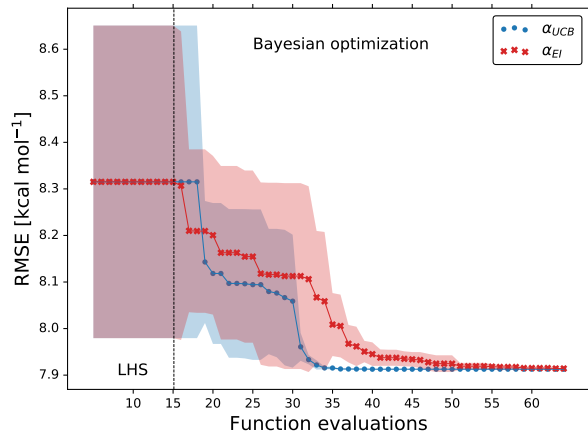


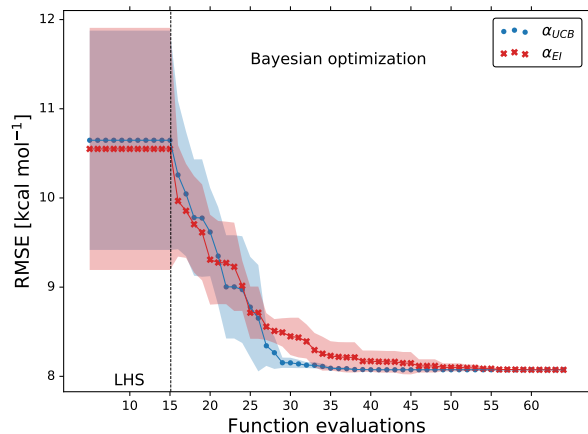
FIG. 1: The averaged minimum observed value of the RMSE for different E_{XC} functionals using BO. For each E_{XC} functional, we ran 5 different initial set of points, $N_0 = 15$, sampled with LHS and the UCB acquisition function with $\kappa = 1$ [42]. The maximum number of points allowed in the BO algorithm was 70, including the initial points. The RMSE was computed using Eq. 1 where R_{m_i} are atomization energies of the G1 molecules [37–39].

optimization, the maximum number of iterations considered was 70 total points. Figure 2 illustrates that with approximately 50 total evaluations of \mathcal{L} , including the initial points, BO found the optimal values of a_0 , a_X and a_C .

The quality of points that are proposed by the acquisition function is a key component in BO [27, 28]. The goal of BO is to circumvent the optimization problem of $f(\mathbf{x})$ to a sequential optimization of $\alpha(\mathbf{x})$, which is a less computational demanding task. In the case of the UCB function, the exploration-exploitation constant κ allows us to probe the space of $f(\mathbf{x})$ without being trapped in a possible local minimum. In the limit where $\sigma(\mathbf{x}) > \mu(\mathbf{x})$, the maximum of α_{UCB} is where the GP model is less certain, allowing us to explore the space. When $\sigma(\mathbf{x}) < \mu(\mathbf{x})$, α_{UCB} allows to explode and converge towards the minimum of $f(\mathbf{x})$ or \mathcal{L} in the case for DF methods. For instance, as shown in Figure 2 we illustrate that as the number of iterations increase in the BO algorithm the GP model becomes more certain about where the minimum of \mathcal{L} is located. Here we present the results for two of the most common E_{XC} functionals, B-LYP and PBE-PBE. For both functionals we optimized the values of a_0 , a_X and a_C using BO. It is important to note that the result of BO is independent of the initial set of points sampled with LHS. The RMSE for the $E_{B,LYP}$ functional is 7.91 kcal mol⁻¹ while for $E_{PBE,PBE}$ is 8.07 kcal mol⁻¹; both results were averaged over 5 different BO optimizations. For $E_{B,LYP}$ the values are $a_0 = 0.1100$, $a_X = 0.8293$ and $a_C = 0.0201$; while for $E_{PBE,PBE}$ $a_0 = 0.1028$,



(a) $E_X=B$ and $E_C=LYP$



(b) $E_X=PBE$ and $E_C=PBE$

FIG. 2: Lowest RMSE for the $E_{B,LYP}$ (upper panel) and $E_{PBE,PBE}$ (lower panel) used BO as a function of the iterations. The symbols and the shaded area are the mean and the standard deviation over 5 different optimizations. For every optimization we considered 15 different initial points. We used two different acquisition functions: \bullet -symbol for the α_{UCB} with $\kappa = 1$ and \times -symbol for the α_{EI} . The RMSE is computed using Eq. 1, where R_{m_i} are atomization energies of the G1 molecules [37–39].

$a_X = 0.8708$ and $a_C = 0.0292$, all obtained using BO. The RMSE for the functionals with their well known versions, B3LYP [45, 46] and PBE0 [3], are 9.48 kcal mol⁻¹ and 11.3 kcal mol⁻¹ respectively.

BO can also be applied to optimize range-separated density functionals [47–50] using non-square type error functions. In Ref. [51] we demonstrated that BO can optimize the parameter in the Yukawa potential between electrons, commonly denoted as γ [47–50]. We used the absolute difference between the highest occupied molecular orbital (HOMO) predicted with LCY-PBE and the

ionization potential for the hydrogen molecule; $\mathcal{L}(\gamma) = |R_{H_2}^{HOMO}(\gamma) - IP|$. We demonstrated that, with a total of 6 points, the value of γ for the *LCY-PBE* functional differed by 0.04 with respect to the reference one, $\hat{\gamma} = 1.2$, obtained with a brute-force search algorithm. We used the UCB acquisition function with $\kappa = 1$ for these calculations [51].

We have shown that BO efficiently optimizes the XC coefficients of a DF model. Some XC functionals tend to better describe some molecular systems than others [52]. This has inspired multiple works where various XC models are compared to each other using different benchmarks [2]. This can also be observed in Figure 1 where the RMSE is lower when the correlation functional is LYP or P86. Taking this into account, we wondered if BO could also help us identify the most appropriate XC functional.

Identifying the most appropriate XC functional is an optimization problem with integer-valued variables,

$$\mathbf{z}^*, \mathbf{x}^* = \arg \min_{\mathbf{z}, \mathbf{x}} f(\mathbf{z}, \mathbf{x}), \quad (11)$$

where \mathbf{z} is an integer vector, $z_i \in \mathbb{Z}^m$.

From Eq. 1 it can be observed that the choice of XC functional is also a parameter of the error function. We define, $\mathbf{z} = [E_X, E_C]$ and $\mathbf{x} = [a_0, a_X, a_C]$. We assigned an integer value to each E_X [43] and E_C [44] functional, e.g. for $E_{PBE, PBE}$ $\mathbf{z} = [5, 4]$ and for $E_{mPW, V5LYP}$ $\mathbf{z} = [3, 6]$.

We also optimized the acquisition function numerically by replacing the continuous values of \mathbf{z} to the closest integer using the floor function e.g. $\lfloor \mathbf{z}_i \rfloor = \lfloor [1.5, 5.8] \rfloor = [1, 5]$, which is $E_{B, VP86}$. We also used the RBF kernel function, Eq. 7, in the GP model used in the BO algorithm. The kernel function describes the similarity between two points. By including E_X and E_C in \mathcal{L} , the dimensionality of the error function changed to $d = 5$; therefore the initial set of points, also sampled with LHS, increased to $N_0 = 25$. For each of the N_0 points the LHS algorithm samples a random XC functional.

We carried out 10 different optimizations with both acquisition functions. Figure 3 illustrates that as the iterations of the algorithm progresses, BO samples different E_{XC} functionals to learn the most accurate XC model. We found that 18 out of 20 times BO selects P86, the most accurate E_C [53]. When using the UCB function, BO can minimize the \mathcal{L} below $7.9 \text{ kcal mol}^{-1}$, Figure 3. We stressed that the BO algorithm learns the correlation between a_0, a_X and a_C with E_X and E_C to select the DF model with the lowest RMSE.

Summary. BO is a powerful optimization method that does not require an analytic expression of the function in order to find the minimum of \mathcal{L} . This makes BO suitable not only for optimizing DF models but also for many other methods and applications in computational physics and chemistry [54]. BO is an iterative algorithm to min-

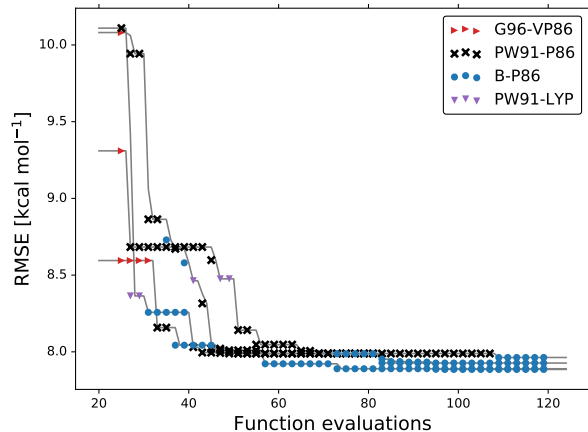


FIG. 3: The minimum RMSE observed as a function of the BO iterations for 4 different optimization using the α_{UCB} with $\kappa = 1$. The symbols represent the different E_{XC} functionals selected by BO at each iteration. We used 25 initial points sampled with LHS for each individual optimization.

imize non-analytic functions and it requires a probabilistic supervised learning model like GP models to construct the acquisition function, which guides the sampling scheme towards the function. The idea of optimizing the XC coefficients of DF models has been proposed before; for example, a search grid method was proposed to optimize the coefficients of B3LYP [7]. This algorithm required three million calculations. Here we have illustrated that BO makes the optimization of hybrid-density models more efficiently. With BO the total number of calculations is a few thousands, $\mathcal{O}(M \times N_{BO}) \approx 2500$, where $M = 41$ is the number of DF calculations for a single evaluation of \mathcal{L} and N_{BO} is the number of iterations BO requires to find the minimum of \mathcal{L} .

The selection between different computational models to simulate a molecular system can also be reformulated into an optimization problem. We have shown that by using the same algorithm we are able to identify the most accurate E_{XC} functional to describe a molecular system. Our work is the first attempt to select and optimize DF models in a more automated manner using an algorithm that can be applied to density functionals with more empirical parameters [55] or more complex ones [19]. This makes the present method particularly valuable for different research fields where computational physics models are optimized using experimental data.

We acknowledge useful discussions with R. V. Krems and R. Ghassemizadeh. This work was supported by the Natural Sciences and Engineering Research Council of Canada (NSERC).

-
- * ravh011@chem.ubc.ca
- [1] R. A. Mata, M. A. Suhm, *Angew. Chem. Int. Ed.* **56**, 11011 (2017).
 - [2] Wolfram Koch, and Max C. Holthausen, *A chemist's guide to density functional theory* (Wiley-VCH, 2000).
 - [3] A. D. Becke, *J. Chem. Phys.* **98**, 5648 (1993).
 - [4] A. D. Becke, *J. Chem. Phys.* **98**, 1372 (1993).
 - [5] F. E. Curtis, and K. Scheinberg, arXiv:1706.10207
 - [6] S. Sra, S. Nowozin, and S. J. Wright, *Optimization for Machine Learning* (The MIT Press, Cambridge, 2012).
 - [7] L. Lu, *Int. J. Quantum Chem.* **115**, 471 (2015).
 - [8] L.-F. Arsenault, A. Lopez-Bezanilla, O. A. von Lilienfeld, and A. J. Millis, *Phys. Rev. B* **90**, 155136 (2014).
 - [9] L.-F. Arsenault, O. A. von Lilienfeld, and A. J. Millis, arXiv:1506.08858.
 - [10] D. Duvenaud, D. Maclaurin, J. Aguilera-Iparraguirre, R. Gómez-Bombarelli, T. Hirzel, Aln Aspuru-Guzik, Ryan P Adams *Adv. Neural Inf. Process. Syst.* **28**, 2224 (2015).
 - [11] R. Gómez-Bombarelli, J. N. Wei, D. Duvenaud, J. M. Hernández-Lobato, B. Sánchez-Lengeling, D. Sheberla, and J. Aguilera-Iparraguirre, T. D. Hirzel, R. P. Adams, and A. Aspuru-Guzik, *ACS Cent. Sci.* **4**, 268 (2018).
 - [12] L. Wang, *Phys. Rev. B* **94**, 195105 (2016).
 - [13] G. Carleo, and M. Troyer, *Science* **355**, 602 (2017).
 - [14] J. Carrasquilla, and R. G. Melko, *Nat. Phys.* **13**, 431 (2017).
 - [15] R. A. Vargas-Hernández, J. Sous, M. Berciu, and R. V. Krems, *Phys. Rev. Lett.* **121**, 255702 (2018).
 - [16] J. C. Snyder, M. Rupp, K. Hansen, K.-R. Müller, and K. Burke *Phys. Rev. Lett.* **108**, 253002 (2012).
 - [17] F. Brockherde, L. Vogt, L. Li, M. E. Tuckerman, K. Burke, and K.-R. Müller, *Nat. Comms.* **8**, 872 (2017).
 - [18] M. Bogojeski, F. Brockherde, L. Vogt-Maranto, L. Li, M. E. Tuckerman, K. Burke, and K.-R. Müller, arXiv:1811.06255
 - [19] J. J. Mortensen, K. Kaasbjerg, S. L. Frederiksen, J. K. Nørskov, J. P. Sethna, and K. W. Jacobsen Bayesian Error Estimation in Density-Functional Theory *Phys. Rev. Lett.* **95**, 216401 (2005).
 - [20] A. J. Medford, J. Wellendorff, A. Vojvodic, F. Studt, F. Abild-Pedersen, K. W. Jacobsen, T. Bligaard, and J. K. Nørskov, *Science* **345**, 6193 (2014).
 - [21] R. Würdemann, H. H. Kristoffersen, M. Moseler, and M. Walter, *J. Chem. Phys.* **142**, 124316 (2015).
 - [22] M. Aldegunde, J. R. Kermode, and N. Zabarar, *J. Comput. Phys.* **311**, 173 (2016).
 - [23] M. Fritz, M. Fernández-Serra, and J. M. Soler *J. Chem. Phys.* **144**, 224101 (2016).
 - [24] L. M. Roch, F. Häse, C. Kreisbeck, T. Tamayo-Mendoza, L. P.-E. Yunker, J. E. Hein, and A. Aspuru-Guzik, *Science Robotics* **3**, 19 (2018).
 - [25] F. Häse, L. M. Roch, C. Kreisbeck, and A. Aspuru-Guzik, *ACS Cent. Sci.* **4**, 1134 (2018).
 - [26] P. B. Wigley, P. J. Everitt, A. van den Hengel, J. W. Bastian, M. A. Sooriyabandara, G. D. McDonald, K. S. Hardman, C. D. Quinlivan, P. Manju, C. C. N. Kuhn, I. R. Petersen, A. N. Luiten, J. J. Hope, N. P. Robins, and M. R. Hush, *Scientific Reports* **6**, 25890 (2016).
 - [27] J. Snoek, H. Larochelle, and R. P. Adams, *Adv. Neur. Inf. Process. Sys.* **25**, 2951(2012).
 - [28] B. Shahriari, K. Swersky, Z. Wang, R. P. Adams, and N. de Freitas, *Proc. IEEE* **104**, 148 (2016).
 - [29] See Supplemental Material “URL will be inserted by publisher” section II.
 - [30] C. E. Rasmussen, and C. K. I. Williams, *Gaussian Processes for Machine Learning* (The MIT Press, Cambridge, 2006).
 - [31] L. Chan, G. Hutchison, and G. Morris, chemrxiv.7228940.v1
 - [32] R. A. Vargas-Hernández, Y. Guan, D. H. Zhang, and R. V. Krems, *New J. Phys.* **21**, 022001(2019).
 - [33] See Supplemental Material “URL will be inserted by publisher” section II.A.
 - [34] J. P. Perdew, M. Ernzerhof, and K. Burke, *J. Chem. Phys.* **105**, 9982 (1996).
 - [35] C. Adamo, and V. Barone, *J. Chem. Phys.* **110**, 6158 (1999).
 - [36] M. Ernzerhof, and G. E. Scuseria, *J. Chem. Phys.* **110**, 5029 (1999).
 - [37] J. A. Pople, M. Head-Gordon, D. J. Fox, K. Raghavachari, and L. A. Curtiss, *J. Chem. Phys.* **90**, 5622 (1989).
 - [38] L. A. Curtiss, C. Jones, G. w. Trucks, K. Raghavachari, and J. A. Pople, *J. Chem. Phys.* **93**, 2537 (1990).
 - [39] D. Feller, and K. A. Peterson, *J. Chem. Phys.* **110**, 8384 (1999).
 - [40] M. J. Frisch, G. W. Trucks, H. B. Schlegel, G. E. Scuseria, M. A. Robb, J. R. Cheeseman, G. Scalmani, V. Barone, B. Mennucci, G. A. Petersson, H. Nakatsuji, M. Caricato, X. Li, H. P. Hratchian, A. F. Izmaylov, J. Bloino, G. Zheng, J. L. Sonnenberg, M. Hada, M. Ehara, K. Toyota, R. Fukuda, J. Hasegawa, M. Ishida, T. Nakajima, Y. Honda, O. Kitao, H. Nakai, T. Vreven, J. A. Montgomery, Jr., J. E. Peralta, F. Ogliaro, M. Bearpark, J. J. Heyd, E. Brothers, K. N. Kudin, V. N. Staroverov, R. Kobayashi, J. Normand, K. Raghavachari, A. Rendell, J. C. Burant, S. S. Iyengar, J. Tomasi, M. Cossi, N. Rega, J. M. Millam, M. Klene, J. E. Knox, J. B. Cross, V. Bakken, C. Adamo, J. Jaramillo, R. Gomperts, R. E. Stratmann, O. Yazyev, A. J. Austin, R. Cammi, C. Pomelli, J. W. Ochterski, R. L. Martin, K. Morokuma, V. G. Zakrzewski, G. A. Voth, P. Salvador, J. J. Dannenberg, S. Dapprich, A. D. Daniels, O. Farkas, J. B. Foresman, J. V. Ortiz, J. Cioslowski, D. J. Fox, Gaussian 09, Revision A.02, Gaussian: Wallingford CT, 2009.
 - [41] M. Stein, *Technometrics* **29**, 143 (1987).
 - [42] See Supplemental Material “URL will be inserted by publisher” Table II.
 - [43] $E_X = [B, PW91, mPW, G96, PBE]$
 - [44] $E_C = [LYP, P86, PW91, VP86, V5LYP]$
 - [45] K. Kim, and K. D. Jordan, *J. Phys. Chem.* **98**, 10089 (1994).
 - [46] P.J. Stephens; F. J. Devlin; C. F. Chabalowski; M. J. Frisch, *J. Phys. Chem.* **98**, 11623 (1994).
 - [47] T. Leininger, H. Stoll, H.-J. Werner, and A. Savin, *Chem. Phys. Lett.* **275**, 151 (1997).
 - [48] H. Iikura, T. Tsuneda, T. Yanai, and K. Hirao, *J. Chern. Phys.* **115**, 3540 (2001).
 - [49] Y. Akinaga, and S. Ten-no, Range-separation by the Yukawa potential in long-range corrected density functional theory with Gaussian-type basis functions. *Chem. Phys. Lett.* **462**, 348 (2008).
 - [50] M. Seth, and T. Ziegler, *J. Chem. Theory Comput.* **8**, 901 (2012).
 - [51] Vargas-Hernández, R. A. (2018). Applications of machine

- learning for solving complex quantum problems (T). PhD Thesis University of British Columbia.
- [52] D. Rappoport, N. R. Crawford, F. Furche and K. Burke, *Approximate Density Functionals: Which Should I Choose?*. In Encyclopedia of Inorganic Chemistry (2009).
- [53] See Supplemental Material “URL will be inserted by publisher” section II.E.
- [54] R. B. Jadrich, B. A. Lindquist, and T. M. Truskett, arXiv:1706.05405
- [55] L. M. Roch, and K. K. Baldrige, *Phys. Chem. Chem. Phys.* **19**, 26191 (2017).

Supplemental Material for
“Bayesian optimization for tuning and selecting hybrid-density functionals”

Rodrigo A. Vargas-Hernández
*Department of Chemistry, University of British Columbia,
Vancouver, British Columbia, Canada, V6T 1Z1*
(Dated: December 15, 2024)

The purpose of this supplemental material is to provide details of the numerical calculations we present in this work and explain the Bayesian optimization algorithm. In section I we present the details of the quantum chemistry calculations, and in section II we introduced introduce Gaussian Process (GP) models and the Bayesian optimization (BO) algorithm.

I. HYBRID-DENSITY FUNCTIONALS

Density functionals (DF) methods are widely use in different fields such as biology, material science and theoretical chemistry. The most common DF methods are the hybrid-density functionals [1, 2],

$$E_{XC}^{acm3} = E_{XC}^{LSD} + a_0(E_X^{exact} - E_X^{LSD}) + a_X(E_X^{GGA} - E_X^{LSD}) + a_C(E_C^{GGA} - E_C^{LSD}), \quad (1)$$

where a_0 , a_X and a_C are adjustable parameters, E_X^{GGA} and E_C^{GGA} are the generalized gradient approximation (GGA) exchange and correlation, and E^{LSD} is the local spin density (LSD) part. a_0 and a_X combine local and non-local treatments of exchange (X) and a_C combines the correlation (C) between LSD and GGA functionals.

The optimization of DF is usually carried by tuning the parameters of DF models that best reproduce experimental data. In this work we considered the *root mean square error* (RMSE) function with respect to the atomization energies of the Gaussian-1 (G1) database [3-5],

$$f = \sqrt{\frac{1}{|M|} \sum_{m_i}^{M} (R_{m_i}^{DFT} - R_{m_i}^{exact})^2}, \quad (2)$$

where $|M|$ is 32 atomization energies considered and $R_{m_i}^{exact}$ is the experimental atomization energy for molecule m_i reported in Table I. $R_{m_i}^{DFT}$ is the atomization energy predicted with a DF model; $R_{m_i}^{DFT}$ is a function of the DF parameters, $R_{m_i}^{DFT} = f(a_0, a_X, a_C)$.

For all calculations the molecular geometries used in the DF calculations were optimized with MP2/6-31G(d), and for all DF calculations we used 6-31G(d). All calculations were performed with the Gaussian 09 suite [6].

TABLE I: Atomization energies D_0 [kcal mol⁻¹] [7].

	Exp.		Exp.
H ₂	103.5	C ₂ H ₂	388.9
LiH	56.0	C ₂ H ₄	531.9
BeH	46.9	C ₂ H ₆	666.3
CH	79.9	CN	176.6
CH ₂ (trip.)	179.6	HCN	301.8
CH ₂ (sing.)	170.6	CO	256.2
CH ₃	289.2	HCO	270.3
CH ₄	392.5	H ₂ CO	357.2
NH	79.0	CH ₃ OH	480.8
NH ₂	170.0	N ₂	255.1
NH ₃	276.7	N ₂ H ₄	405.4
OH	101.3	NO	150.1
H ₂ O	219.3	O ₂	118.0
HF	135.2	H ₂ O ₂	252.3
Li ₂	24.0	F ₂	36.9
LiF	137.6	CO ₂	381.9

II. BAYESIAN OPTIMIZATION

Bayesian optimization is a sequential search algorithm designed to find the minimum/maximum of a non-analytic function, denoted here as f , without requiring the gradient of the function [8, 9],

$$\mathbf{x}^* = \arg \min_{\mathbf{x}} f(\mathbf{x}). \quad (3)$$

BO is constructed using two ingredients, a probabilistic model that approximates f and an acquisition function that quantifies the informational gain if f were to be evaluated in a new point. Here we denoted \mathcal{F} as the probabilistic model.

A. GP

In this work we used Gaussian process (GP) models as the probabilistic model that approximates f , $\mathcal{F} \approx f$. GP models are robust supervised learning models that assume the data is Gaussian distributed [10]. The prediction of a GP model is a normal distribution characterized by a mean $\mu(\cdot)$ and a standard deviation $\sigma(\cdot)$, given as

$$\mu(\mathbf{x}_*) = K(\mathbf{x}_*, X)^\top [K(X, X) + \sigma_n^2 I]^{-1} \mathbf{y} \quad (4)$$

$$\sigma(\mathbf{x}_*) = K(\mathbf{x}_*, \mathbf{x}_*) - K(\mathbf{x}_*, X)^\top [K(X, X) + \sigma_n^2 I]^{-1} K(X, \mathbf{x}_*), \quad (5)$$

where K is the design or covariance matrix and its matrix elements are computed using a kernel function, $K_{i,j} = k(\mathbf{x}_i, \mathbf{x}_j)$. For this work we only considered the *radial basis function* (RBF) kernel,

$$k_{RBF}(\mathbf{x}_i, \mathbf{x}_j) = \exp\left(-\frac{1}{2}(\mathbf{x}_i - \mathbf{x}_j)^\top M(\mathbf{x}_i - \mathbf{x}_j)\right), \quad (6)$$

where

$$M = \begin{pmatrix} \ell_1 & & 0 \\ & \ddots & \\ 0 & & \ell_d \end{pmatrix}, \quad (7)$$

and ℓ_i is the length-scale parameter for each dimension of \mathbf{x} . We described all ℓ_d s jointly as denoted as θ , $\theta = [\ell_1, \dots, \ell_d]$. The parameters of the kernel function, θ , are optimized by maximizing the marginal log-likelihood,

$$\log p(\mathbf{y}|X, \theta) = -\frac{1}{2}\mathbf{y}^\top K(X, X)^{-1}\mathbf{y} - \frac{1}{2}\log |K(X, X)| - \frac{N}{2}\log(2\pi), \quad (8)$$

where N is the total number of points in \mathcal{D} and $|K(X, X)|$ is the determinant of the design matrix.

B. Acquisition function

The acquisition function, denoted as α , is the function that guides the sampling scheme in BO towards the minimum/maximum of f . An acquisition function can only be constructed using the information obtained from \mathcal{F} . There are several acquisition functions, in this work we only used two; the expected improvement (EI) and the upper confidence bound (UCB),

$$\alpha_{EI}(\mathbf{x}) = (\mu(\mathbf{x}) - y_{max})\Phi(z(\mathbf{x}; y_{max})) + \sigma(\mathbf{x})\phi(z(\mathbf{x}; y_{max})) \quad (9)$$

$$\alpha_{UCB}(\mathbf{x}) = \mu(\mathbf{x}) + \kappa\sigma(\mathbf{x}), \quad (10)$$

where $\mu(\mathbf{x})$ and $\sigma(\mathbf{x})$ are the mean and the standard deviation from a GP model, Eqs. (4-5). For EI, $\Phi(\cdot)$ is the normal cumulative distribution and $\phi(\cdot)$ is the normal probability distribution, $z(\mathbf{x}; y_{min}) = (\mu(\mathbf{x}) - y_{min})/\sigma(\mathbf{x})$, and y_{min} is the minimum value observed in the training data, $y_{min} = \arg \min \mathbf{y}$. The UCB function has a hyper-parameter κ known as the exploration-exploitation constant. κ controls the sampling scheme of α_{UCB} towards exploratory moves or exploitation moves.

C. BO algorithm

In this section we present how BO algorithm finds the minimum of an error function like Eq. 2 for DF models. For illustrative purposes we minimized the single adjustable parameter a_0 of the *PBE0* functional where, $a_X = 1 - a_0$ and $a_C = 1$ [11–13]. We only considered the atomization energies in Table I, the Gaussian-1 (G1) database [3–5]. The first step in the BO algorithm is to gather some data to train a GP model. The training data was gathered by randomly sample three values for a_0 , $x_{1:3} \sim U(0, 1)$, and compute $f(a_0, a_X = 1 - a_0, a_C = 1)$. We used latin hyper cube sampling (LHS) algorithm [14] to sample the initial points when we jointly optimized all three DF parameters. The second step

is to train a GP model to approximate f . Then we optimized the acquisition function constructed with the trained GP model to select the next query point where f will be evaluated, $f(\mathbf{x}_{N+1})$. The optimization of the acquisition function can be done numerically. Once we evaluate f at \mathbf{x}_{N+1} we update the GP model and carried this procedure sequentially until we converge to the minimum/maximum of f . Algorithm 1 and Figure 1 illustrate the BO algorithm to optimize hybrid-DF models. In Figure 1 we can observe that with only 6 evaluations of f , BO found that the minimum of f is for $a_0 = 0.1502$; the RMSE = 10.08 kcal mol⁻¹. For this calculations we used the UCB acquisition function with $\kappa = 1$.

Algorithm 1 Bayesian optimization

Input: Acquisition function $\alpha(\cdot)$, black-box function $f(\cdot)$, data set \mathcal{D} .

- 1: **for** $n = 1, 2, \dots$, **do**
 - 2: Optimize the acquisition function,

$$\mathbf{x}_{n+1} = \arg \max_{\mathbf{x}} \alpha(\mathbf{x}, \mathcal{D})$$
 - 3: Evaluate $f(\mathbf{x}_{n+1})$.
 - 4: Augment data $\mathcal{D}_{n+1} = \{\mathcal{D}_n, (\mathbf{x}_{n+1}, f(\mathbf{x}_{n+1}))\}$.
 - 5: Update model.
-

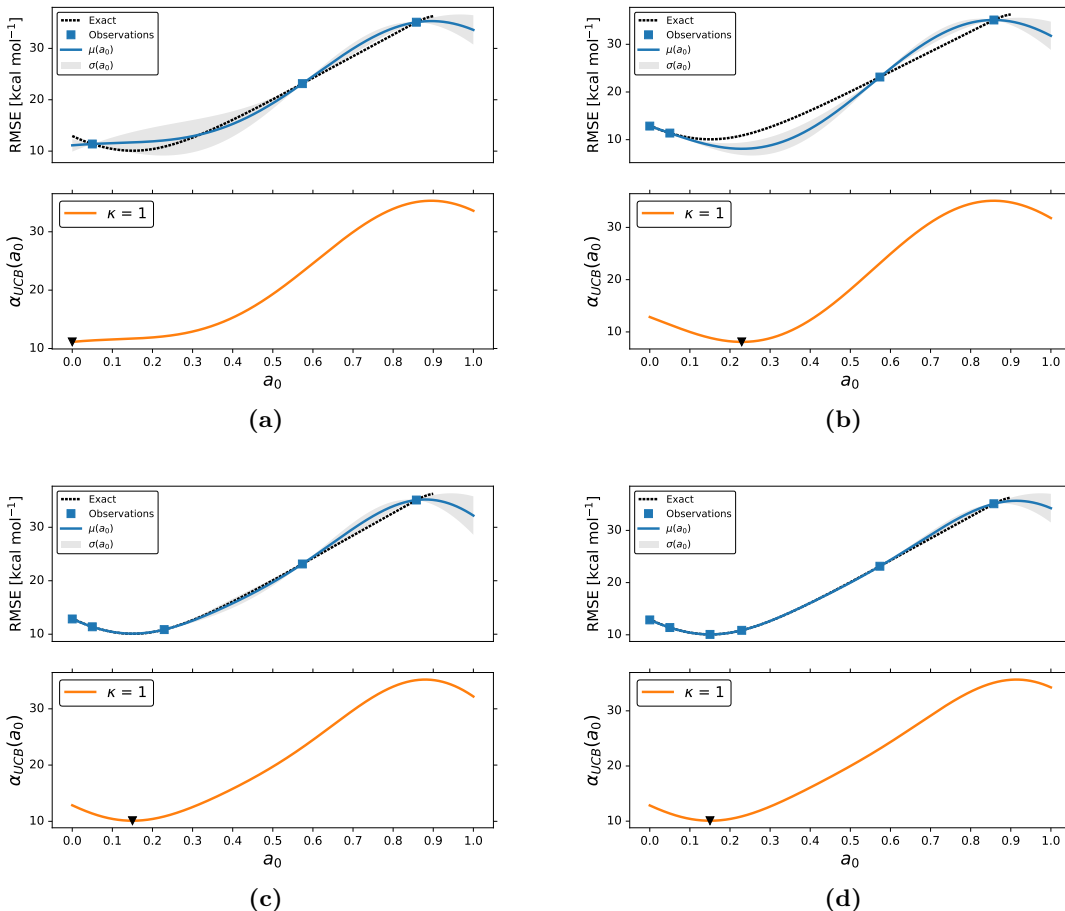


Fig. SM 1: Each figure is an iteration of the BO algorithm, we present present 4 iterations. (Upper panels) The solid-blue curve is the mean of the GP model and shaded area is the standard deviation of the GP model. The markers are the training data used to construct the GP model. The black-dashed line is the exact form or f . The orange curves in the lower panels are the UCB acquisition function, Eq. 10, with $\kappa = 1$. The marker (\blacktriangledown) represents the maximum of α_{UCB} which is the proposed point by the BO algorithm.

D. Results for ACM3 functionals

TABLE II: The RMSE of various E_{XC} optimized with BO and the UCB acquisition function with $\kappa = 1$. RMSEs are reported in [kcal mol⁻¹] [7]. The RMSE was computed with respect to atomization energy of G1 molecules [3–5], Table I. We sampled 15 initial points with the LHS algorithm.

E_X	E_C	a_0	a_X	a_C	RMSE	E_X	E_C	a_0	a_X	a_C	RMSE	E_X	E_C	a_0	a_X	a_C	RMSE
B	LYP	0.1055	0.8416	0.0001	7.911	PW91	VP86	0.0766	0.9406	0.0001	8.132	G96	PW91	0.0834	0.7327	0.0001	8.130
		0.1028	0.8484	0.0001	7.913			0.0768	0.9395	0.0001	8.132			0.0849	0.7301	0.0001	8.130
		0.1100	0.8293	0.0201	7.912			0.0790	0.9339	0.0001	8.132			0.0854	0.7295	0.0001	8.130
		0.1112	0.8299	0.0162	7.913			0.0768	0.9399	0.0001	8.132			0.0839	0.7318	0.0001	8.130
		0.1078	0.8374	0.0001	7.913			0.0736	0.9476	0.0001	8.132			0.0840	0.7320	0.0001	8.130
B	P86	0.1156	0.7842	0.0001	7.887	PW91	V5LYP	0.1147	0.8844	0.2830	8.158	G96	PBE	0.0838	0.7327	0.0001	8.130
		0.1153	0.7845	0.0001	7.887			0.0957	0.9008	0.1392	8.123			0.0844	0.7319	0.0010	8.130
		0.1178	0.7802	0.0001	7.887			0.0931	0.9086	0.1226	8.121			0.0841	0.7312	0.0001	8.130
		0.1157	0.7837	0.0001	7.887			0.0985	0.9028	0.1663	8.123			0.0852	0.7283	0.0001	8.130
		0.1153	0.7839	0.0001	7.887			0.0931	0.9090	0.1174	8.121			0.0836	0.7325	0.0001	8.130
B	PW91	0.0853	0.7864	0.0001	8.047	mPW	LYP	0.1151	0.8808	0.1056	7.957	G96	VP86	0.0757	0.7459	0.0004	8.168
		0.0856	0.7857	0.0001	8.047			0.1046	0.9064	0.0001	7.966			0.0782	0.7425	0.0001	8.168
		0.0852	0.7865	0.0001	8.047			0.1228	0.8642	0.1283	7.959			0.0783	0.7426	0.0001	8.168
		0.0856	0.7858	0.0001	8.047			0.1142	0.8829	0.0933	7.957			0.0773	0.7435	0.0001	8.168
		0.0849	0.7870	0.0001	8.047			0.1201	0.8720	0.0658	7.961			0.0777	0.7463	0.0001	8.169
B	PBE	0.0855	0.7870	0.0001	8.047	mPW	P86	0.1130	0.8476	0.0001	7.924	G96	V5LYP	0.0803	0.7378	0.0001	8.168
		0.0855	0.7860	0.0001	8.047			0.1139	0.8457	0.0001	7.924			0.0751	0.7471	0.0001	8.168
		0.0861	0.7847	0.0001	8.047			0.1124	0.8499	0.0001	7.924			0.0682	0.7563	0.0001	8.174
		0.0902	0.7771	0.0001	8.048			0.1136	0.8465	0.0001	7.924			0.0784	0.7415	0.0007	8.168
		0.0860	0.7856	0.0001	8.047			0.1120	0.8497	0.0001	7.924			0.0010	0.5006	1.0000	8.168
B	VP86	0.0830	0.7917	0.0001	8.080	mPW	PW91	0.0832	0.8507	0.0001	8.060	PBE	LYP	0.1145	0.9536	0.0001	8.033
		0.0789	0.7981	0.0001	8.079			0.0834	0.8482	0.0001	8.060			0.1287	0.9136	0.1413	8.014
		0.0759	0.8077	0.0001	8.081			0.0849	0.8451	0.0001	8.060			0.1311	0.9075	0.1445	8.014
		0.0786	0.7997	0.0001	8.079			0.0838	0.8481	0.0001	8.060			0.1324	0.9040	0.1497	8.014
		0.0786	0.7994	0.0001	8.079			0.0829	0.8506	0.0001	8.060			0.1333	0.9024	0.1466	8.014
B	V5LYP	0.0767	0.8030	0.0001	8.079	mPW	PBE	0.0828	0.8503	0.0001	8.060	PBE	P86	0.1247	0.8845	0.0001	7.984
		0.0774	0.8028	0.0001	8.079			0.0820	0.8506	0.0001	8.060			0.1148	0.9057	0.0001	7.988
		0.0806	0.7945	0.0001	8.079			0.0731	0.8718	0.0001	8.063			0.1328	0.8676	0.0001	7.986
		0.0830	0.7892	0.0001	8.080			0.0826	0.8510	0.0001	8.060			0.1241	0.8868	0.0001	7.984
		0.0790	0.7987	0.0001	8.079			0.0831	0.8496	0.0001	8.060			0.1251	0.8839	0.0001	7.984
PW91	LYP	0.1266	0.9247	0.1964	8.021	mPW	VP86	0.0772	0.8624	0.0001	8.092	PBE	PW91	0.0895	0.8997	0.0001	8.072
		0.1274	0.9269	0.1869	8.021			0.0763	0.8647	0.0001	8.092			0.0898	0.8986	0.0001	8.072
		0.1173	0.9430	0.1382	8.029			0.0768	0.8617	0.0001	8.092			0.0921	0.8937	0.0001	8.071
		0.1277	0.9242	0.1983	8.021			0.0768	0.8647	0.0001	8.092			0.0994	0.8752	0.0001	8.074
		0.1288	0.9189	0.1877	8.022			0.0776	0.8617	0.0001	8.092			0.0921	0.8935	0.0001	8.071
PW91	P86	0.1139	0.9218	0.0001	7.993	mPW	V5LYP	0.0865	0.8483	0.0706	8.090	PBE	PBE	0.0924	0.8920	0.0001	8.071
		0.1149	0.9184	0.0001	7.993			0.0820	0.8558	0.0494	8.090			0.0910	0.8986	0.0001	8.072
		0.0989	0.9516	0.0088	8.009			0.0876	0.8458	0.0702	8.090			0.1028	0.8708	0.0292	8.079
		0.0819	1.0000	0.0001	8.040			0.0841	0.8505	0.0472	8.090			0.0923	0.8933	0.0001	8.071
		0.1161	0.9167	0.0001	7.993			0.0864	0.8447	0.0435	8.089			0.0913	0.8957	0.0001	8.071
PW91	PW91	0.0838	0.9254	0.0034	8.100	G96	LYP	0.1031	0.7865	0.0001	7.909	PBE	VP86	0.0861	0.9079	0.0001	8.098
		0.0935	0.9004	0.0099	8.103			0.1079	0.7814	0.0001	7.912			0.0838	0.9128	0.0001	8.098
		0.0820	0.9293	0.0001	8.100			0.1024	0.7881	0.0001	7.909			0.0864	0.9068	0.0001	8.098
		0.0838	0.9236	0.0001	8.100			0.1052	0.7826	0.0001	7.910			0.0909	0.8927	0.0001	8.100
		0.0831	0.9254	0.0001	8.100			0.1015	0.7890	0.0001	7.909			0.0844	0.9109	0.0001	8.098
PW91	PBE	0.0826	0.9268	0.0001	8.100	G96	P86	0.1146	0.7286	0.0001	7.896	PBE	V5LYP	0.0949	0.8918	0.0721	8.097
		0.0814	0.9304	0.0001	8.100			0.1129	0.7325	0.0001	7.896			0.0955	0.8891	0.0594	8.097
		0.0821	0.9284	0.0001	8.100			0.1130	0.7321	0.0001	7.896			0.0881	0.9038	0.0282	8.097
		0.0826	0.9274	0.0140	8.100			0.1131	0.7320	0.0001	7.896			0.0858	0.9073	0.0001	8.098
		0.0534	1.0000	0.0001	8.138			0.1122	0.7334	0.0001	7.896			0.1013	0.8760	0.0272	8.103

E. Integer-valued variables in BO

The selection of the exchange, E_X , and correlation, E_C , functionals determines the accuracy in the prediction of physical properties with DF models. In this work we present that BO can optimize the DF parameters and select the most optimal forms for the exchange and correlation functionals. For this procedure we considered the same loss function as before, Eq. 2, and include the possibility to select different E_X and E_C ,

$$f = f(E_X, E_C, a_0, a_X, a_C). \quad (11)$$

We consider six different exchange and five different correlation functionals; $E_X = [\text{B}, \text{PW91}, \text{mPW}, \text{G96}, \text{PBE}]$ and $E_C = [\text{LYP}, \text{P86}, \text{PW91}, \text{VP86}, \text{V5LYP}]$. We label each E_X and E_C with different sequential integer numbers; for example for the mPW-P86 functional $E_X = 2$ and $E_C = 1$. The points proposed in each of the BO algorithm described one E_X and E_C functional and the DF parameters, $[\mathbf{z}, \mathbf{x}] = [[E_X, E_C], a_0, a_X, a_C]$. During the optimization of the acquisition function we replaced the continuous values of the first two components of \mathbf{x} for the with the closest integers using the floor function,

$$[\mathbf{z}, \mathbf{x}] = [[1.45], [2.35], 0.15, 0.8, 0.01] = [1, 2, 0.15, 0.8, 0.01] = [\text{PW91}, \text{PW91}, 0.15, 0.8, 0.0]. \quad (12)$$

The 25 initial points were also sampled using the LHS algorithm. Each point is a 5-dimensional vector which first two components are the E_X and E_C . We also used the floor function to convert them into integer numbers. Figure 2 illustrates that BO can also be used to optimize the DF parameters and identify the optimal E_X and E_C functionals.

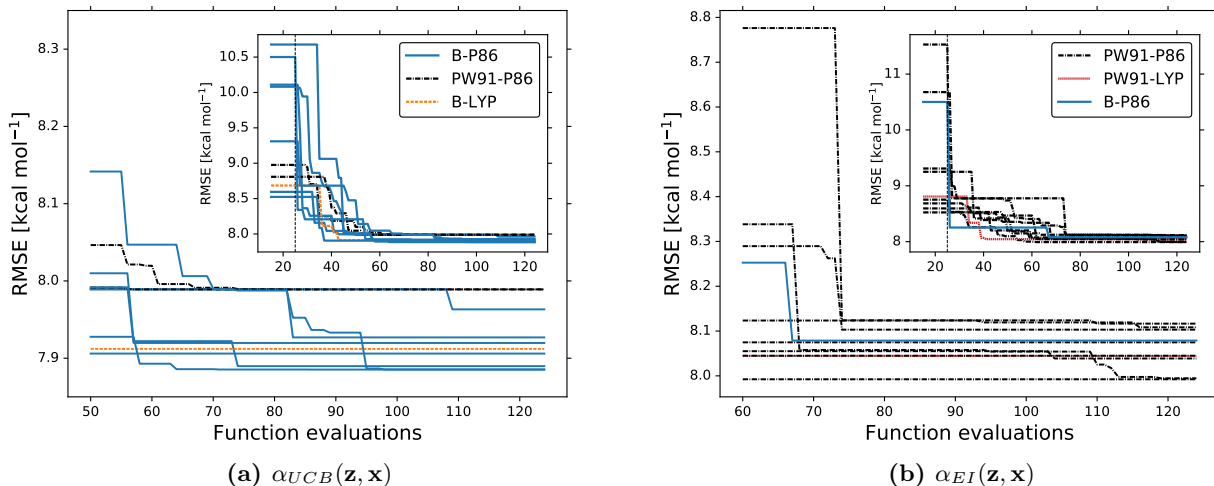


Fig. SM 2: The minimum RMSE observed value as a function of the iterations in the BO algorithm. The curves indicate the E_{XC} with the lowest RMSE found by BO; BP86 for solid blue curves (—), PW91P86 for dot-dashed black curves (— · —), BLYP for dashed orange curves (— · —) and PW91LYP for red dotted curves (· · ·). For each BO optimization we used 25 initial points sampled with LHS and two different acquisition functions, α_{UCB} with $\kappa = 1$ (upper panel) and α_{EI} (lower panel). The RMSE is computed using Eq. 2, where R_{m_i} are atomization energies of the G1 molecules [3–5].

-
- [1] A. D. Becke, *J. Chem. Phys.* **98**, 5648 (1993).
 - [2] A. D. Becke, *J. Chem. Phys.* **98**, 1372 (1993).
 - [3] J. A. Pople, M. Head-Gordon, D. J. Fox, K. Raghavachari, and L. A. Curtiss, *J. Chem. Phys.* **90**, 5622 (1989).
 - [4] L. A. Curtiss, C. Jones, G. w. Trucks, K. Raghavachari, and J. A. Pople, *J. Chem. Phys.* **93**, 2537 (1990).
 - [5] D. Feller, and K. A. Peterson, *J. Chem. Phys.* **110**, 8384 (1999).
 - [6] M. J. Frisch, G. W. Trucks, H. B. Schlegel, G. E. Scuseria, M. A. Robb, J. R. Cheeseman, G. Scalmani, V. Barone, B. Mennucci, G. A. Petersson, H. Nakatsuji, M. Caricato, X. Li, H. P. Hratchian, A. F. Izmaylov, J. Bloino, G. Zheng, J. L.

Sonnenberg, M. Hada, M. Ehara, K. Toyota, R. Fukuda, J. Hasegawa, M. Ishida, T. Nakajima, Y. Honda, O. Kitao, H. Nakai, T. Vreven, J. A. Montgomery, Jr., J. E. Peralta, F. Ogliaro, M. Bearpark, J. J. Heyd, E. Brothers, K. N. Kudin, V. N. Staroverov, R. Kobayashi, J. Normand, K. Raghavachari, A. Rendell, J. C. Burant, S. S. Iyengar, J. Tomasi, M. Cossi, N. Rega, J. M. Millam, M. Klene, J. E. Knox, J. B. Cross, V. Bakken, C. Adamo, J. Jaramillo, R. Gomperts, R. E. Stratmann, O. Yazyev, A. J. Austin, R. Cammi, C. Pomelli, J. W. Ochterski, R. L. Martin, K. Morokuma, V. G. Zakrzewski, G. A. Voth, P. Salvador, J. J. Dannenberg, S. Dapprich, A. D. Daniels, O. Farkas, J. B. Foresman, J. V. Ortiz, J. Cioslowski, D. J. Fox, Gaussian 09, Revision A.02, Gaussian: Wallingford CT, 2009.

- [7] A. D. Becke, *J. Chem. Phys.* **96**, 2155 (1992).
- [8] J. Snoek, H. Larochelle, and R. P. Adams, *Adv. Neur. Inf. Process. Sys.* **25**, 2951(2012).
- [9] B. Shahriari, K. Swersky, Z. Wang, R. P. Adams, and N. de Freitas, *Proc. IEEE* **104**, 148 (2016).
- [10] C. E. Rasmussen, and C. K. I. Williams, *Gaussian Processes for Machine Learning* (The MIT Press, Cambridge, 2006).
- [11] J. P. Perdew, M. Ernzerhof, and K. Burke, *J. Chem. Phys.* **105**, 9982 (1996).
- [12] C. Adamo, and V. Barone, *J. Chem. Phys.* **110**, 6158 (1999).
- [13] M. Ernzerhof, and G. E. Scuseria, *J. Chem. Phys.* **110**, 5029 (1999).
- [14] M. Stein, *Technometrics* **29**, 143 (1987).